Clim Dyn (2011) 37:915–931
DOI 10.1007/s00382-010-0868-1

Albedo enhancement of marine clouds to counteract global warming: impacts on the hydrological cycle

G. Bala · Ken Caldeira · Rama Nemani · Long Cao · George Ban-Weiss · Ho-Jeong Shin

Received: 6 February 2010 / Accepted: 11 June 2010 / Published online: 24 June 2010

Abstract Recent studies have shown that changes in solar radiation affect the hydrological cycle more strongly than equivalent CO_2 changes for the same change in global mean surface temperature. Thus, solar radiation management "geoengineering" proposals to completely offset global mean temperature increases by reducing the amount of absorbed sunlight might be expected to slow the global water cycle and reduce runoff over land. However, proposed countering of global warming by increasing the albedo of marine clouds would reduce surface solar radiation only over the oceans. Here, for an idealized scenario, we analyze the response of temperature and the hydrological cycle to increased reflection by clouds over the ocean using an atmospheric general circulation model coupled to a mixed layer ocean model. When cloud droplets are reduced in size over all oceans uniformly to offset the temperature increase from a doubling of atmospheric CO_2, the global-mean precipitation and evaporation decreases by about 1.3% but runoff over land increases by 7.5% primarily due to increases over tropical land. In the model, more reflective marine clouds cool the atmospheric column over ocean. The result is a sinking motion over oceans and upward motion over land. We attribute the increased runoff over land to this increased upward motion over land when marine clouds are made more reflective. Our results suggest that, in contrast to other proposals to increase planetary albedo, offsetting mean global warming by reducing marine cloud droplet size does not necessarily lead to a drying, on average, of the continents. However, we note that the changes in precipitation, evaporation and P-E are dominated by small but significant areas, and given the highly idealized nature of this study, a more thorough and broader assessment would be required for proposals of altering marine cloud properties on a large scale.

Keywords Climate change · Global warming · Geoengineering · Solar radiation management · Marine cloud-albedo enhancement · Hydrological cycle

Electronic supplementary material The online version of this article (doi:10.1007/s00382-010-0868-1) contains supplementary material, which is available to authorized users.

G. Bala
Divecha Center for Climate Change,
Indian Institute of Science, Bangalore 560 012, India

K. Caldeira · L. Cao · G. Ban-Weiss · H.-J. Shin
Department of Global Ecology, Carnegie Institution,
260 Panama Street, Stanford, CA 94305, USA

R. Nemani
NASA Ames Research Center, Moffett Field,
CA 94035, USA

G. Bala (✉)
Center for Atmospheric and Oceanic Sciences,
Indian Institute of Science, Bangalore 560 012, India
e-mail: bala.gov@gmail.com

1 Introduction

Enhancing the albedo of marine stratocumulus clouds via increasing cloud condensation nuclei (CCN) has been proposed as a "solar radiation management (SRM)" geoengineering scheme to counteract global warming (Bower et al. 2006; Latham 1990, 2002; Latham et al. 2008). It has been suggested that CCN can be increased by spraying a fine seawater mist into the remote marine atmospheric boundary layer (Latham 1990). More CCN will increase the number of cloud droplets while reducing the droplet size and hence increase the total droplet surface area of the

clouds and cloud albedo (Twomey 1977). This scheme differs from other SRM schemes (Angel 2006; Bala 2009; Crutzen 2006; Early 1989; NAS 1992; Seifritz 1989; Teller et al. 1997) in that the reduction in solar radiation is applied nearly exclusively over the oceans rather than nearly uniformly over both land and oceans.

In a recent study (Bala et al. 2008), it was shown that the ratio of changes in rainfall to changes in temperature is greater when caused by variations in solar radiation than when they are caused by variations in CO_2 levels. This occurs, in part, because changes in solar radiation directly affect the amount of energy at the surface available to drive evaporation. Furthermore, absorbed solar radiation tends to heat the atmosphere from below, decreasing vertical stability, and promoting precipitation. In contrast, CO_2 absorption of longwave radiation reaches a maximum in the upper troposphere, where it cannot directly drive evaporation, and can contribute to increased vertical stability and suppress precipitation. Therefore, changes in rainfall are more sensitive to variations in solar radiation than to equivalent changes in CO_2 levels (Andrews et al. 2009; Bala et al. 2009). Because of this differing hydrological sensitivity to solar and CO_2 forcing it has been suggested that insolation reductions sufficient to offset the entirety of global-scale temperature increases would lead to a decrease in global mean precipitation and decrease in runoff over land (Bala et al. 2008; Trenberth and Dai 2007).

Past climate modelling studies of SRM schemes (Govindasamy and Caldeira 2000; Govindasamy et al. 2003, 2002; Lunt et al. 2008; Matthews and Caldeira 2007; Rasch et al. 2008; Robock et al. 2008; Tilmes et al. 2009) have represented geoengineering approaches that do not fundamentally distinguish between land and ocean, such as placing reflecting materials at the L1 Lagrange point between the sun and earth (the point where the gravitational forces of earth and sun cancel each other), and injecting sulphate aerosols into the stratosphere.

Persistent marine stratus clouds off the west coasts of the continents such as South America, North America and Africa would be likely targets for a cloud seeding program to modify climate. Recent climate modelling of such selective seeding (Jones et al. 2009) has shown that 35% of the radiative forcing due to current levels of greenhouse gases could be offset by stratocumulus modification. Transient coupled model simulations in the same study suggest that geoengineering of the three aforementioned stratocumulus areas could delay the simulated global warming by about 25 years. These simulations also indicate that, while some areas experience increases in precipitation and net primary productivity, sharp decreases are simulated in South America, with particularly detrimental impacts on the Amazon rain forest. This study concludes that while some areas benefit from geoengineering, there are significant areas where the response could be detrimental with implications for the practical applicability of such a scheme.

Reflecting more sunlight from clouds over the ocean can affect precipitation in at least two important ways: (1) Less sunlight would reach the ocean surface, and hence less energy would be available to evaporate seawater. Therefore, the water vapour content over oceans and its advection to land would tend to decline. (2) Since the oceans would be cooled relative to the continents, there would be a tendency to favor flows of moist air from ocean to land, increasing precipitation on land. Thus, it is not obvious if the slowdown of the global hydrological cycle (Bala et al. 2008), especially as seen on land will occur for SRM schemes that increase the albedo of marine clouds. In this study, we attempt to estimate the effect of these two mechanisms using a general circulation model that has explicit representation of cloud microphysics and its effects on the radiative budget of the planet.

The main goal of this study is to improve our understanding of the basic mechanisms by which decreasing droplet size in marine clouds affects the climate system. We address this issue by performing idealized simulations in which cloud droplet size is reduced for all clouds above all oceans around the globe. We focus on conceptual understanding of the fundamental properties of the climate system when negative solar forcing is applied over the ocean areas alone to counter global warming. In particular, we seek to understand changes in land hydrology. The climate model description is given in Sect. 2 and the simulations are discussed in Sect. 3. Results are presented in Sect. 4 and Sect. 5 has concluding discussions.

2 The model

The atmosphere model used here, CAM3.5 (Collins et al. 2006), has a horizontal resolution of 1.9° latitude by 2.5° longitude and 26 layers in the vertical dimension. We use the finite volume (FV) dynamical core configuration for atmospheric transport. To allow for interactions between the atmosphere and ocean, the model is coupled to a simple slab-ocean/thermodynamic sea-ice model. For the standard configuration of the model, the effective cloud droplet size over land and ocean is 8 and 14 μm, respectively. The droplet size over sea ice is the same as over the ocean surface. For the slab ocean, the mixed layer depths were prescribed to climatological values, and the ocean heat transport was prescribed as derived from the net energy flux over the ocean surface in a climatological simulation performed with prescribed sea surface temperature. The atmosphere model is coupled with a land surface model,

CLM3.5 (Oleson et al. 2008), which represents the land surface by sixteen different plant functional types (PFT) and simulates a number of biophysical processes for each PFT, such as stomatal physiology and photosynthesis, interactions of energy and water fluxes with vegetation canopy and soil, and the surface hydrology.

3 Simulations

We perform three 70-year simulations using the coupled CAM3.5/CLM3.5 model: (1) a control "1 × CO_2" simulation with an atmospheric CO_2 concentration of 400 ppm meant to approximately represent the present-day atmospheric CO_2 concentration; (2) a "2 × CO_2" simulation in which CO_2 concentration is doubled to 800 ppm; (3) a geoengineering simulation "2 × CO_2 + CCN" in which CO_2 concentration is doubled to 800 ppm and the effective radius of the cloud droplets over the ocean is reduced from 14 to 11.5 μm. No changes were made to the effective droplet size for ice clouds. For the 2 × CO_2 + CCN experiment, we alter the effective radius of cloud liquid water droplets over ocean areas in the microphysics package of the model since the shortwave optical properties of clouds depend on the effective radius of the cloud droplets.

Besides the climate change caused by longwave radiative effects of CO_2, there is possible impacts of the physiological effect of CO_2 on plant stomatal conductance called 'the CO_2 physiological forcing' which can result in land surface climate change. For example, there are many studies that discuss the possible impacts of CO_2 physiological forcing on land surface warming and runoff (Betts et al. 2007; Boucher et al. 2009; Cao et al. 2009; Doutriaux-Boucher et al. 2009; Gedney et al. 2006). To restrict our investigation to radiative effects, we have turned off the CO_2 physiological effect by prescribing the same CO_2 concentration (400 ppmv) to the land model in all our experiments.

The choice of 11.5 μm for 2 × CO_2 + CCN is based on results from a series of simulations in which the droplet radius for marine clouds was reduced to 12, 11.5, 11, and 10 μm. The case with 11.5 μm, designated 2 × CO_2 + CCN, has the least departure in global mean surface temperature from the control case (Table 1): this is the simulation analyzed in this paper. There is a residual warming of 0.4 K over land, and the mean-ocean surface temperature decreases by 0.1 K in this case (Table 1). We found that the experiment with 12 μm, designated 2 × CO_2 + CCN12, had the least departure in global-mean precipitation relative to the control case but it had a global-mean warming of 0.6 K (Table 1). The global-mean temperature change is nearly mitigated in 2 × CO_2 + CCN but global-mean precipitation is decreased relative to the control. In the 2 × CO_2 + CCN12 case, precipitation change is nearly mitigated but global-mean temperature is increased relative to the control. This is in agreement with our earlier finding that an alternation in solar forcing might offset temperature changes or hydrological changes from equivalent greenhouse gas changes, but could not perfectly cancel both at once (Bala et al. 2008). Changes in 2 × CO_2 + CCN12, relative to 1 × CO_2, differ from the corresponding changes in 2 × CO_2 + CCN for other variables as well and mostly scale with the global-mean surface temperature change of 0.6 K in the 2 × CO_2 + CCN12.

We find no statistically significant trend in model results after 30 years of simulated time, and therefore we have used the last 40 years (out of 70 years) of each simulation for equilibrium climate change analysis. The last 40 years of global- and annual-mean surface temperature of the control simulation have a standard deviation of 0.2 K and a drift of only -5.8×10^{-6} K per year.

4 Results

Here, we adopt the following approach in discussing our results. First, in each of following sub section, we briefly describe changes resulting from a doubling of atmospheric CO_2 content (i.e., results for 2 × CO_2 minus results for 1 × CO_2). Next, we describe changes resulting from a decrease of cloud droplet size over the oceans (i.e., 2 × CO_2 + CCN − 2 × CO_2). Lastly, we examine the net effect of increased CO_2 with smaller marine cloud droplets (i.e., 2 × CO_2 + CCN − 1 × CO_2).

4.1 Radiative forcing

First, it is useful to compare the radiative forcing from doubling of CO_2 to that due to the reduction in marine cloud droplet size over the oceans. Hence, we repeated the three experiments (1 × CO_2, 2 × CO_2 and 2 × CO_2 + CCN) discussed in the previous section but with prescribed climatological sea surface temperatures (SST) for 40-year periods in order to make an estimate of the radiative forcing using Hansen's "fixed-SST method" (Hansen et al. 2005). In this method, the radiative forcing is estimated as the change in the net radiative fluxes at the top of the atmosphere after the stratosphere, troposphere and land surface are allowed to adjust. Radiative forcing can be also estimated from the slab-ocean simulations by performing a regression of changes in the top of the atmosphere net radiative flux with surface temperature change (Gregory et al. 2004). We use Hansen's method here because the spatial pattern of forcing is directly available in this

Table 1 Global-and annual-mean changes in key climate variables

Variable	$1 \times CO_2$	$2 \times CO_2$ minus $1 \times CO_2$	$2 \times CO_2 + CCN$ minus $2 \times CO_2$	$2 \times CO_2 + CCN$ minus $1 \times CO_2$	$2 \times CO_2 + CCN12$ minus $1 \times CO_2$
Surface temperature (global, K)	288.20 ± 0.02[a]	2.44 ± 0.03	−2.39 ± 0.03	0.06 ± 0.03	0.59 ± 0.03
Surface temperature (land mean, K)	282.30 ± 0.02	2.90 ± 0.04	−2.53 ± 0.04	0.37 ± 0.03	0.92 ± 0.03
Surface temperature (ocean mean, K)	290.64 ± 0.02	2.26 ± 0.03	−2.33 ± 0.03	−0.07 ± 0.03	0.46 ± 0.03
Precipitation (global, mm/day, %)[b,e]	2.894 ± 0.002	5.03 ± 0.08	−6.01 ± 0.07	−1.28 ± 0.08	0.18 ± 0.07
Precipitation (Land, mm/day, %)[b,e]	2.478 ± 0.007	5.84 ± 0.30	−2.19 ± 0.23	3.52 ± 0.33	4.11 ± 0.35
Precipitation (ocean, mm/day, %)[b,e]	3.065 ± 0.003	4.75 ± 0.12	−7.29 ± 0.08	−2.89 ± 0.11	−1.13 ± 0.11
Evaporation (land, mm/day, %)[b,e,f]	1.668 ± 0.003	5.87 ± 0.21	−4.05 ± 0.19	1.58 ± 0.21	2.95 ± 0.17
Evaporation (Ocean, mm/day, %)[b,e]	3.399 ± 0.002	4.86 ± 0.08	−6.41 ± 0.06	−1.86 ± 0.07	−0.38 ± 0.08
P-E (land, mm/day, %)[b,c,e]	0.810 ± 0.006	5.80 ± 0.88	1.63 ± 0.58	7.52 ± 0.87	6.50 ± 1.01
P-E (ocean, mm/day, %)[b,c,e]	−0.334 ± 0.002	−5.80 ± 0.85	−1.64 ± 0.58	−7.54 ± 0.85	−6.51 ± 1.00
Omega (land, mb day^{-1})[d]	0.17 ± 0.08	0.45 ± 0.09	−1.61 ± 0.09	−1.16 ± 0.11	−0.75 ± 0.10
Omega (ocean, mb day^{-1})	−0.01 ± 0.03	−0.17 ± 0.04	0.63 ± 0.03	0.46 ± 0.04	0.30 ± 0.14
Precipitable water (global, kg m^{-2}, %)[b,e]	25.23 ± 0.04	16.77 ± 0.22	−13.93 ± 0.16	0.50 ± 0.18	4.06 ± 0.18
Precipitable water (land, kg m^{-2}, %)[b,e]	19.49 ± 0.04	17.61 ± 0.28	−12.89 ± 0.22	2.46 ± 0.25	5.91 ± 0.22
Precipitable water (ocean, kg m^{-2}, %)[b,e]	27.60 ± 0.04	16.52 ± 0.21	−14.24 ± 0.15	−0.08 ± 0.17	3.52 ± 0.19
Sea ice area (million km^2, %)[b,e]	19.19 ± 0.09	−33.54 ± 0.63	52.14 ± 1.08	1.11 ± 0.71	−7.04 ± 0.77

[a] Uncertainty is given by the standard error computed from 40 annual means. The standard error is corrected for autocorrelation (Zwiers and von Storch 1995)

[b] Percentage changes relative to the control

[c] Percentage changes are relative to the absolute value in the control. Land has positive P-E in the control and ocean has negative P-E

[d] Omega refers to the pressure velocity (negative is upward motion) at the 510.45 mb hybrid-sigma level, and it reflects approximately the vertical motion in the mid-troposphere

[e] The first unit is for the mean values in the $1 \times CO_2$ case, and the second unit is for the changes given in 3rd, 4th, 5th and 6th columns

[f] Global-mean change in evaporation is equal to global-mean change in precipitation and hence not shown in the table

method while an ensemble of simulations is needed to obtain a reliable estimate of the forcing using the regression method. A comparison of these methods is available in the literature (Bala et al. 2009; Gregory and Webb 2008; Hansen et al. 2005).

The radiative forcing is spatially nearly uniform when CO_2 is doubled and is statistically significant at the 1% level around the globe (Fig. 1, top panel). The global, land, and ocean mean forcings are 3.56 ± 0.04, 3.42 ± 0.08, and 3.62 ± 0.04 Wm^{-2}, respectively (Table 2). The climate sensitivity in this case is 1.46 Wm^{-2}/K^{-1}. The forcing is mostly confined to the oceans when marine cloud droplet size is decreased (Fig. 1, middle panel); in this case, the global, land, and ocean mean values are −3.20 ± 0.04, −0.89 ± 0.07, and −4.16 ± 0.04 Wm^{-2}, respectively. There is radiative forcing over land in this case even though forcing was applied only over the oceans because both the troposphere and land surface have been allowed to adjust. The spatial pattern (Fig. 1) shows that the forcing is large and significant over the oceans but small and mostly not significant over land. The climate sensitivity in this case is 1.34 Wm^{-2}/K^{-1} which is only about 10% lower than in the case when CO_2 is doubled. This suggests that climate sensitivity is roughly constant and the radiative forcing concept is capable of predicting the global mean temperature change, at least for the two types of forcings studied here (Forster et al. 2000; Hansen et al. 1997, 2005).

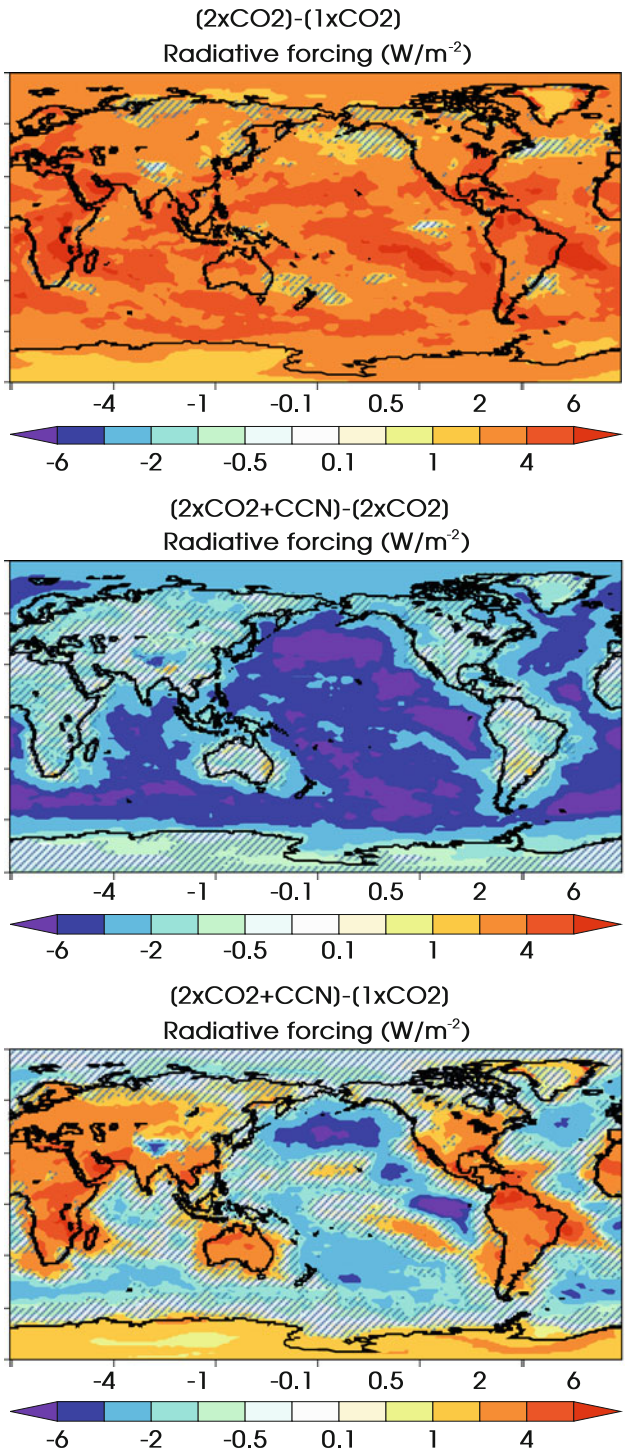

Fig. 1 Radiative forcing calculated using the "fixed-SST method" (Hansen et al. 2005) for doubled atmospheric CO_2 content ($2 \times CO_2 - 1 \times CO_2$), reduced marine cloud droplet size ($2 \times CO_2 + CCN - 2 \times CO_2$) and the case with both the effects included ($2 \times CO_2 + CCN - 1 \times CO_2$). The hatching indicates regions where the changes are not significant at the 1% level. Significance level is estimated using a Student *t* test with a sample of 40 annual means and standard error corrected for autocorrelation (Zwiers and von Storch 1995)

When the forcings are combined, there is residual positive forcing over land and negative forcing over the oceans (Fig. 1, bottom panel) because the forcings due to doubling of CO_2 and the reduction of marine cloud droplet size sum up to produce the combined forcing. The global, land, and ocean mean forcings simulated in the combined case is 0.35 ± 0.04, 2.52 ± 0.08 and -0.54 ± 0.04 Wm^{-2}, respectively (Table 2) while a summation of forcings from doubling CO_2 and reduction of marine cloud droplet size would give 0.36 ± 0.06, 2.53 ± 0.10, -0.54 ± 0.06 Wm^{-2}, respectively. The large non-zero land mean forcing in the combined case mainly arises from the non uniform (ocean vs. land) application of forcing in $2 \times CO_2 + CCN$. The spatial pattern of forcing (Fig. 1) shows that the forcing over oceans in this case is small and not significant over most places at the 1% significance level.

4.2 Global mean changes

Results for a doubling of atmospheric CO_2 are typical of other climate models (IPCC 2007). For a doubling of atmospheric CO_2 from 400 to 800 ppm, the model yields a global mean warming of 2.44 ± 0.03 K, with a 2.90 ± 0.04 K warming over land and 2.26 ± 0.03 K over ocean (Table 1). The ratio of land to sea warming is 1.28, which is comparable to the results obtained in an intercomparision of IPCC AR4 models which, for a doubling of CO_2, showed a range of 1.18–1.58 for slab-ocean equilibrium simulations (Sutton et al. 2007). The enhanced warming over land is not simply a transient effect: it is also present in equilibrium conditions (Andrews et al. 2009; Sutton et al. 2007). Previous studies have attributed the land/sea contrast in warming to differing lapse rates over land and oceans, the nonlinear increase of water vapor with temperature (Joshi et al. 2008), and a reduction in boundary layer relative humidity over land triggered by the CO_2-physiological effect and associated cloud feedbacks (Doutriaux-Boucher et al. 2009). The turning-off of the CO_2-physiological effect in our experiments is a possible cause for the lower ratio of land/sea warming contrast in this study; Table S1 suggests that low-level relative humidity over land actually increases when climate warms in this model.

Primarily because of increases in absolute humidity with warmer temperatures, global precipitation increases $5.03 \pm 0.08\%$ ($5.84 \pm 0.30\%$ over land and $4.75 \pm 0.12\%$ over ocean). There is a decrease in mean large scale upward motion over land regions: however, increases in precipitation over land could be due to increases in atmospheric water vapor content over land (Table 1). In steady

Table 2 Global- and annual-mean "fixed-SST" radiative forcing

Adjusted radiative forcing	2 × CO_2 minus 1 × CO_2	2 × CO_2 + CCN minus 2 × CO_2	2 × CO_2 + CCN minus 1 × CO_2
Global (Wm^{-2})	3.56 ± 0.04*	−3.20 ± 0.04	0.35 ± 0.04
Land mean (Wm^{-2})	3.42 ± 0.08	−0.89 ± 0.07	2.52 ± 0.08
Ocean mean (Wm^{-2})	3.62 ± 0.04	− 4.16 ± 0.04	−0.54 ± 0.04

* Uncertainty is given by the standard error computed from 40 annual means. The standard error is corrected for autocorrelation (Zwiers and von Storch 1995)

state, runoff from land to ocean is equal to the net atmospheric water vapour transport from ocean to land and is also equal to precipitation minus evaporation over land. Runoff from land to ocean increases by 5.8 ± 0.9% relative to 1 × CO_2. The global-mean precipitation increases 2.0% per degree global-mean warming.

Decreasing the size of droplets in marine clouds from 14 to 11.5 μm causes the modeled 2 × CO_2 + CCN climate to cool by 2.39 ± 0.03 K, with a 2.53 ± 0.04 K cooling over land and 2.33 ± 0.03 K cooling over ocean relative to 2 × CO_2 (Table 1). A previous idealized modelling study (Forster et al. 2000) found a similar result: larger response over land than over the oceans even though radiative forcing is applied only over the oceans. However, the ratio of land to sea temperature change is reduced in this case to 1.09 largely because the droplet size is reduced only for marine clouds (i.e., the negative radiative forcing is applied only over the oceans). It may be counterintuitive that reflecting more sunlight over the ocean cools the land more than the ocean, but this occurs, as stated earlier, because of differing lapse rates over oceans and land and the nonlinear dependence of water vapor on temperature (Joshi and Gregory 2008; Joshi et al. 2008); on average, the atmosphere over the ocean has a moist adiabatic lapse rate in the vertical but over the land has a lapse rate that is between a dry and moist adiabatic lapse rates. Because of these differing lapse rates, we notice a larger temperature response in upper levels over the oceans than over land (Fig. 2); the lapse rate change is larger for the atmosphere over oceans.

Decreasing droplet size also causes the global precipitation to decrease by 6.01 ± 0.07% which is a 2.6% decrease in precipitation per degree cooling. In this model, global-mean precipitation changes are about 30% more sensitive to solar forcing than to an equivalent CO_2 forcing (Andrews et al. 2009; Bala et al. 2009, 2008).

In the 2 × CO_2 + CCN simulation, relative to the 2 × CO_2 case, albedo of clouds is enhanced only over ocean areas. The resulting spatial contrast in radiative forcing (Fig. 1) leads to a "monsoonal" circulation with descending motion over the oceans and ascending motion over land (Table 1; Figs. 3, 4). Because we increase cloud albedo over the ocean, the vertically integrated air mass over the ocean cools more than the air mass over land. The

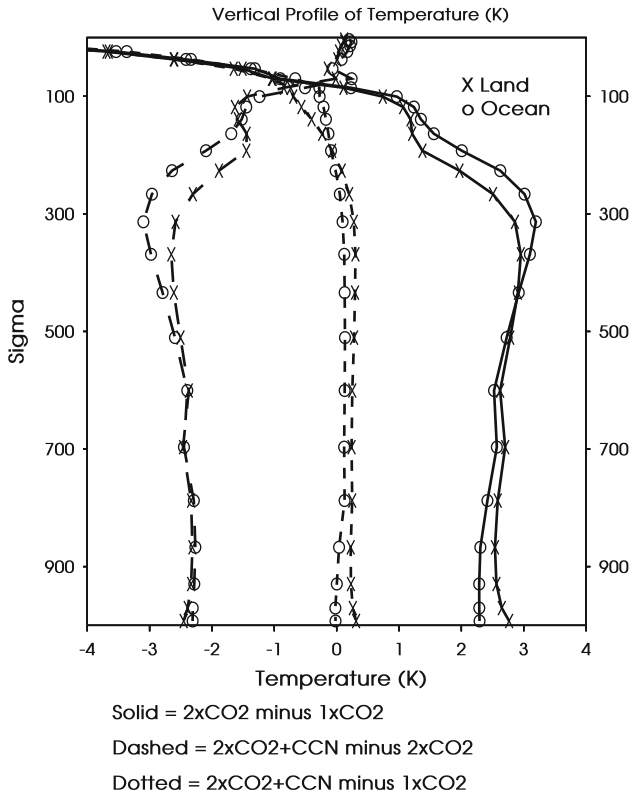

Fig. 2 Vertical profile of the changes in land-mean, and ocean-mean temperatures. Changes are shown for the case with doubled atmospheric CO_2 content (2 × CO_2 − 1 × CO_2), reduced marine cloud droplet size (2 × CO_2 + CCN − 2 × CO_2) and the case with both the effects included (2 × CO_2 + CCN − 1 × CO_2). The vertical coordinate is the model's sigma coordinate and no vertical interpolation to pressure coordinate is performed because several land grid points are below the topography for levels below 700 mb. We find that the lapse rate changes are larger for the temperature profiles over the oceans than over land because air parcels follow the moist adiabats over the oceans and nearly follow the dry adiabats over land (Joshi et al. 2008)

resulting density change causes an increase in net transport of air from land to ocean at pressures less than about 400 mb and an increase in net transport of air from ocean to land below this level, with an increase in net upward flow of air over land at around 400 mb and an increase in net downward flow of air over the oceans at this pressure level (Fig. 3). This monsoonal flow tends to increase water vapor transport from ocean to land. Further discussion of this

monsoonal circulation is provided in the Sect. 4.4. Land surface temperatures cool more than ocean surface temperatures (even when forced by changing sea surface temperatures) despite the vertically integrated air mass over ocean cooling more than the vertically integrated air mass over land. This behaviour occurs because moist oceanic adiabats steepen more than drier land adiabats in response to cooling (Joshi et al. 2008).

Evaporation over land decreases (Table 1), but the magnitude of the reduction in precipitation over land is smaller due to the strengthened monsoonal circulation and hence there is more runoff. Precipitation decreases by 7.29 ± 0.08% over oceans and by only 2.19 ± 0.23% over land (Table 1). These contrasts in precipitation responses are associated with the mean sinking motion over the oceans and rising motion over land (Table 1; Figs. 3, 4); we attribute the smaller decrease in precipitation over land to the upward air motion over land. The precipitation decrease on land is only 0.9% per degree cooling. Evaporation over ocean decreases by 6.41 ± 0.06% and by 4.05 ± 0.19% over land because of a cooler climate: the larger decrease over oceans is the result of enhancing the cloud albedo only over the oceans (Fig. 1). Runoff over land does not decrease (as would be the case if cloud seeding was the exact opposite of doubling CO_2) but instead increases by 1.6%. This increase in runoff over land with smaller marine cloud droplets indicates that implementation of the Latham (1990) proposal might tend to lead to a moistening, on average, of soils.

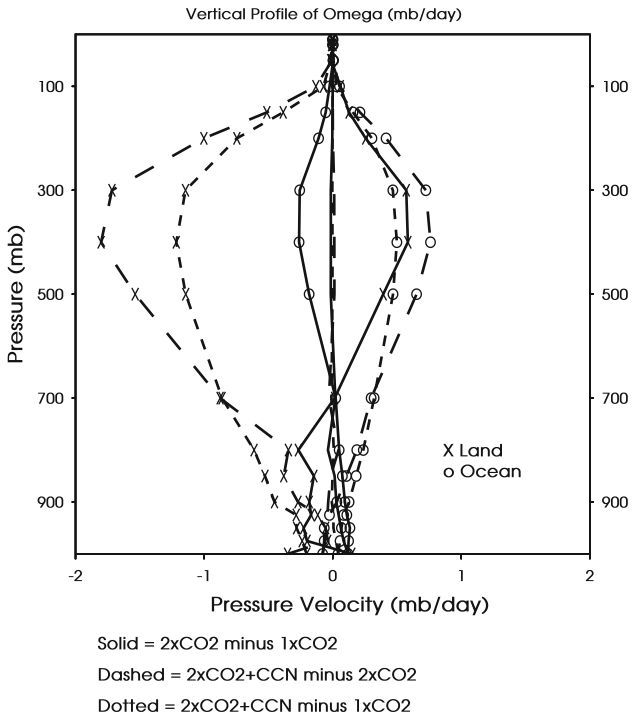

Fig. 3 Vertical profile of the changes in global-mean (*no marker*), land-mean (*cross*), and ocean-mean (*circle*) pressure velocity (*omega*). Negative values in omega changes represent increases in upward motion and vice versa. Changes are shown for the case with doubled atmospheric CO_2 content ($2 \times CO_2 - 1 \times CO_2$), reduced marine cloud droplet size ($2 \times CO_2 + CCN - 2 \times CO_2$) and the case with both the effects included ($2 \times CO_2 + CCN - 1 \times CO_2$). The data is vertically interpolated to the pressure levels because omega is equivalent to mass flux and interpretation in terms of mass conservation is made easier in the pressure coordinate system. When CO_2 concentration is increased, there is a slight upward motion over ocean and downward motion over land. When marine cloud droplet size is reduced, large increases in the upward motion over land and downward motion over ocean are induced

For the combined effects of increased CO_2 content and decreased marine cloud droplet size (i.e., the $2 \times CO_2 + CCN$ simulation relative to the $1 \times CO_2$ simulation), there is a residual warming of 0.37 ± 0.03 K over land and a decrease in mean-ocean surface temperature of 0.07 ± 0.03 K relative to the $1 \times CO_2$ case (Table 1).The global-mean precipitation is decreased by 1.28 ± 0.08%, which is consistent with conclusions based on studies involving globally reduced absorption of sunlight (Bala et al. 2008): for a specified amount of temperature change or radiative forcing, one should expect to see a greater impact on the hydrological cycle from changes in sunlight than for changes in atmospheric CO_2 content (Andrews et al. 2009; Bala et al. 2008). This difference is a fundamental property of the climate system. The precipitation decrease in the $2 \times CO_2 + CCN$ (relative to $1 \times CO_2$) is mainly over the oceans (−2.89 ± 0.11%): over land, mean precipitation increases by 3.52 ± 0.33%. These contrasts in precipitation responses are associated with the mean sinking motion over the oceans and rising motion over land (Table 1; Figs. 3, 4). The increase in land precipitation is in contrast to decreases observed for geoengineering simulations with a uniform reduction in sunlight over both land and oceans (Bala et al. 2008).

Overall runoff from land, equivalent in steady state to precipitation minus evaporation, increases over land by 7.52 ± 0.87% (Table 1), which implies that increasing albedo of marine clouds may produce an increase in runoff over land. A corresponding decrease in precipitation minus evaporation is observed over ocean areas where changes in evaporation exceed changes in precipitation. In summary, we find that enhancing the albedo of marine clouds decreases evaporation more than precipitation over the ocean and increases precipitation more than evaporation over the land. This increase in runoff over land is attributed to enhanced upward motion over land and should be contrasted with previous modelling studies in which decreases in solar insolation resulted in a decrease in runoff (Bala et al. 2008).

Changes in net shortwave fluxes at the surface are <1 Wm^{-2} when atmospheric CO_2 content is doubled (Table S1). However, a decrease in the size of droplets in

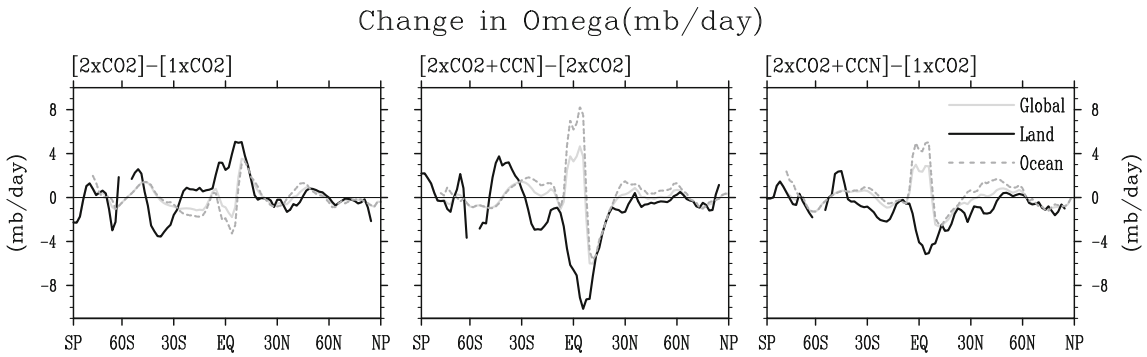

Fig. 4 Changes in zonal- and annual-mean omega (pressure velocity) at the hybrid sigma level of 508.45. This level approximately corresponds to the 500 mb pressure surface. Negative values in omega changes represent increases in upward motion and vice versa. Changes are shown for the case with doubled atmospheric CO_2 content ($2 \times CO_2 - 1 \times CO_2$), reduced marine cloud droplet size ($2 \times CO_2 + CCN - 2 \times CO_2$) and the case with both the effects included ($2 \times CO_2 + CCN - 1 \times CO_2$) for land (*black*), ocean (*dashed*) and all regions (*grey*). Note the increase in upward motion over tropical land regions in the case with reduced cloud droplet size and in the case with doubled CO_2 content and reduced droplet size, indicating the monsoonal effect due to reducing the droplet size of marine clouds

marine clouds from 14 to 11.5 μm ($2 \times CO_2 + CCN - 2 \times CO_2$) leads to a decrease in surface net shortwave fluxes by 3.67 ± 0.07 Wm^{-2} over the ocean area, and by 2.71 ± 0.05 Wm^{-2} in the global-mean. Changes in cloud fraction are not the primary cause for these large changes in shortwave fluxes (Table S1): cloud fraction changes are <1% and the magnitude of changes is very similar to that in the $2 \times CO_2$ case, which does not show large changes in shortwave fluxes. It is the change in cloud albedo via the decreased cloud droplet radius that leads to a large drop in the shortwave fluxes.

In the case where atmospheric CO_2 content is increased and marine cloud droplet size is decreased (i.e., $2 \times CO_2 + CCN - 1 \times CO_2$), changes in the top of the atmosphere (TOA) net shortwave fluxes are similar and are almost identical to changes in shortwave cloud forcing (Table S1): changes in the global-mean TOA shortwave fluxes are nearly exclusively the result of changes in cloudy regions; TOA shortwave fluxes in clear-sky regions are nearly unchanged. The decreases in TOA net shortwave fluxes of 3.44 ± 0.05 and 4.39 ± 0.08 Wm^{-2} for the global and ocean averages are associated with planetary albedo increases of 1.02 ± 0.02 and 1.29 ± 0.03%, respectively (Table S1). A smaller increase in TOA albedo (0.35 ± 0.03%) is associated with increased cloudiness over land (Table S1), probably due to increased water vapour transport from ocean areas to land. The large decrease in TOA longwave fluxes of 3.4 Wm^{-2} in the $2 \times CO_2 + CCN$ case relative to the $1 \times CO_2$ case is necessary for net TOA energy balance and is approximately indicative of the longwave radiative forcing in the $2 \times CO_2$ case (Table S1, and 2); $2 \times CO_2 + CCN$, to a good approximation, is a case with two radiative forcings (increased longwave fluxes into the climate system due to doubled CO_2 and reduced shortwave fluxes due to albedo enhancement of clouds) balancing each other with no temperature change relative to the control case.

4.3 Spatial pattern of changes

Surface temperature change for a doubling of atmospheric CO_2 is significant at the 1% level over all grid points over the globe (Fig. 5). The changes are larger over land and high-latitude regions, in agreement with the published literature (IPCC 2007). Cooling of similar magnitude at the same significance level is simulated when the cloud droplet size is reduced ($2 \times CO_2 + CCN - 2 \times CO_2$). Precipitable water changes are significant at the 1% level for every vertical grid column in the model in both cases. We found that the water vapour changes approximately follow the Clausius–Clayperon relationship (~7% change per degree change in temperature; Allen and Ingram 2002; Held and Soden 2006); the pattern of precipitable water changes follows the temperature change pattern. Although significant over 51 and 54% of the globe, changes in temperature and precipitable water are much smaller in the case with both increased CO_2 content and reduced droplet size ($2 \times CO_2 + CCN - 1 \times CO_2$), suggesting substantial mitigation of CO_2-induced climate change in terms of temperature and atmospheric water vapor content.

For the doubled CO_2 case, vertically integrated total cloud fraction increases in the polar region and in the tropics, and decreases in mid latitudes and subtropics (Fig. 6). Similar patterns with comparable magnitude but opposite sign are simulated for the case with reduced cloud droplet size suggesting that cloud changes in the later case result mainly from climate changes rather than as a direct result of the decrease in cloud droplet size. TOA albedo, an

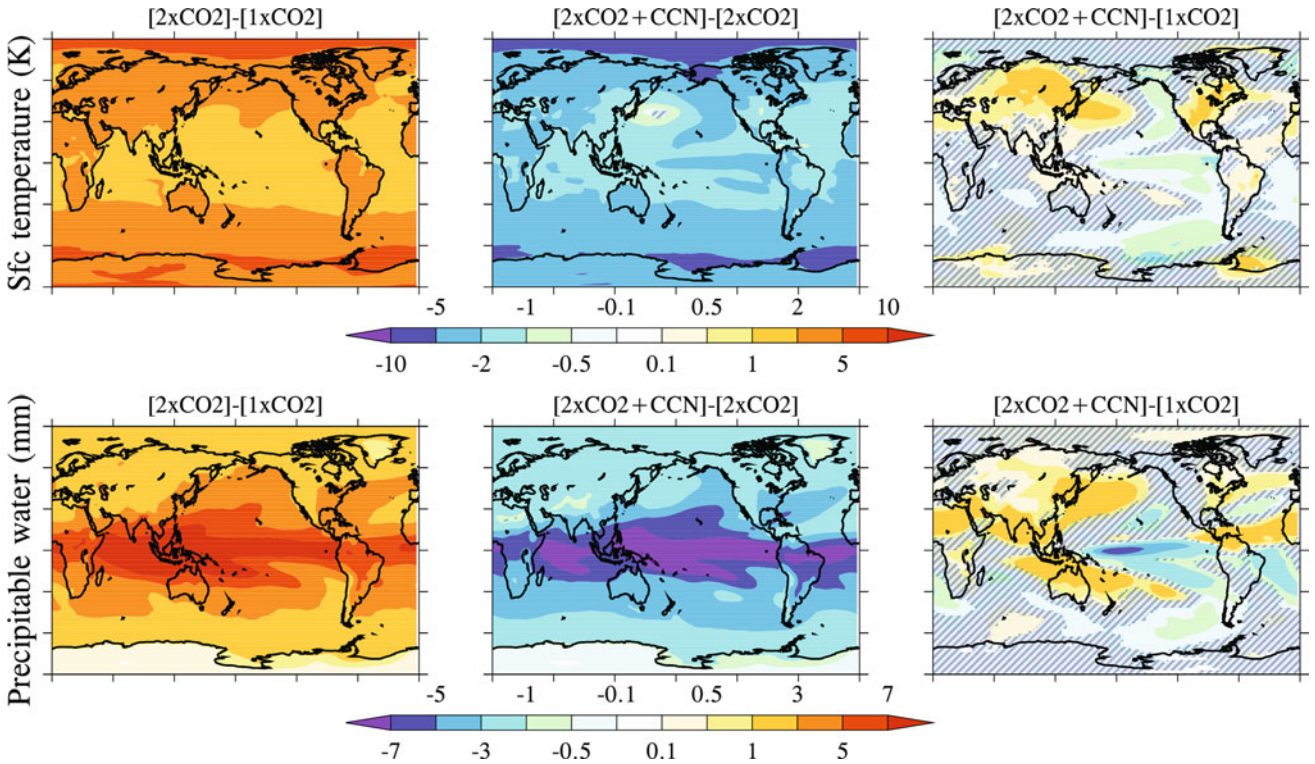

Fig. 5 Changes in global- and annual-mean surface temperature and precipitable water due to increase in CO_2 content ($2 \times CO_2 - 1 \times CO_2$), reduction in marine cloud droplet size ($2 \times CO_2 + CCN - 2 \times CO_2$) and a combination of both increased CO_2 content and reduced droplet size ($2 \times CO_2 + CCN - 1 \times CO_2$). The hatching indicates regions where the changes are not significant at the 1% level. Significance level is estimated using a Student *t* test with a sample of 40 annual means and standard error corrected for autocorrelation (Zwiers and von Storch 1995)

indicator for the magnitude of reflected sunlight from the atmospheric column shows a large decrease in the polar region in the $2 \times CO_2$ case because of decreased sea ice cover (Table 1). Cloud fraction increases in this region (Fig. 6) and hence it is unlikely to be the cause for albedo decrease. TOA albedo increases in tropical regions where the cloudiness has increased. Because the albedo of marine clouds are enhanced when droplet size is reduced, magnitudes of the TOA albedo changes are much larger when marine cloud droplet size is reduced ($2 \times CO_2 + CCN - 2 \times CO_2$) than when atmospheric CO_2 is doubled; the increase is as high as 5% in the eastern tropical pacific when marine cloud droplet size is reduced. The correlation between changes in TOA albedo and surface net shortwave fluxes for the doubled CO_2 case and the case with reduced droplet size are 0.95 and 0.92, respectively.

The spatial pattern of hydrological changes is shown in Fig. 7. When atmospheric CO_2 content is doubled, precipitation increases in the tropics and high latitudes, and decreases in the subtropics; in the zonal mean, wet places get wetter and dry regions get drier (Held and Soden 2006). Evaporation changes do not mirror changes in precipitation (Held and Soden 2006) and increases in evaporation occur almost everywhere when atmospheric CO_2 is doubled. For the case with reduced droplet size for marine clouds ($2 \times CO_2 + CCN - 2 \times CO_2$), the pattern of precipitation and evaporation changes is similar to the doubled CO_2 case but with opposite sign; this indicates that reducing marine cloud droplet size may tend to cause wet regions to become drier and dry regions to become wetter. As a result of reducing cloud droplet size, evaporation decreases almost everywhere.

The pattern of precipitation minus evaporation changes resembles the changes in precipitation (Held and Soden 2006) in both the doubled CO_2 case and the case with reduced droplet size. Runoff increases over most of the land areas in the doubled CO_2 case and decreases in the case with reduced droplet size. However, note that mean runoff over land increases in the later case (Table 1) largely because of the large runoff increases in the tropics. Zonal-mean vertical velocity shows increases in upward motion over tropical land (Fig. 4) in association with the increase in runoff. There is some suggestion of regional negative P-E when marine cloud droplet size is reduced: significant drying over Southern Europe and southern Amazonia is simulated. When both the effects are combined ($2 \times CO_2 + CCN - 1 \times CO_2$), there is decline in P and E over ocean and increase over land (Table 1), and

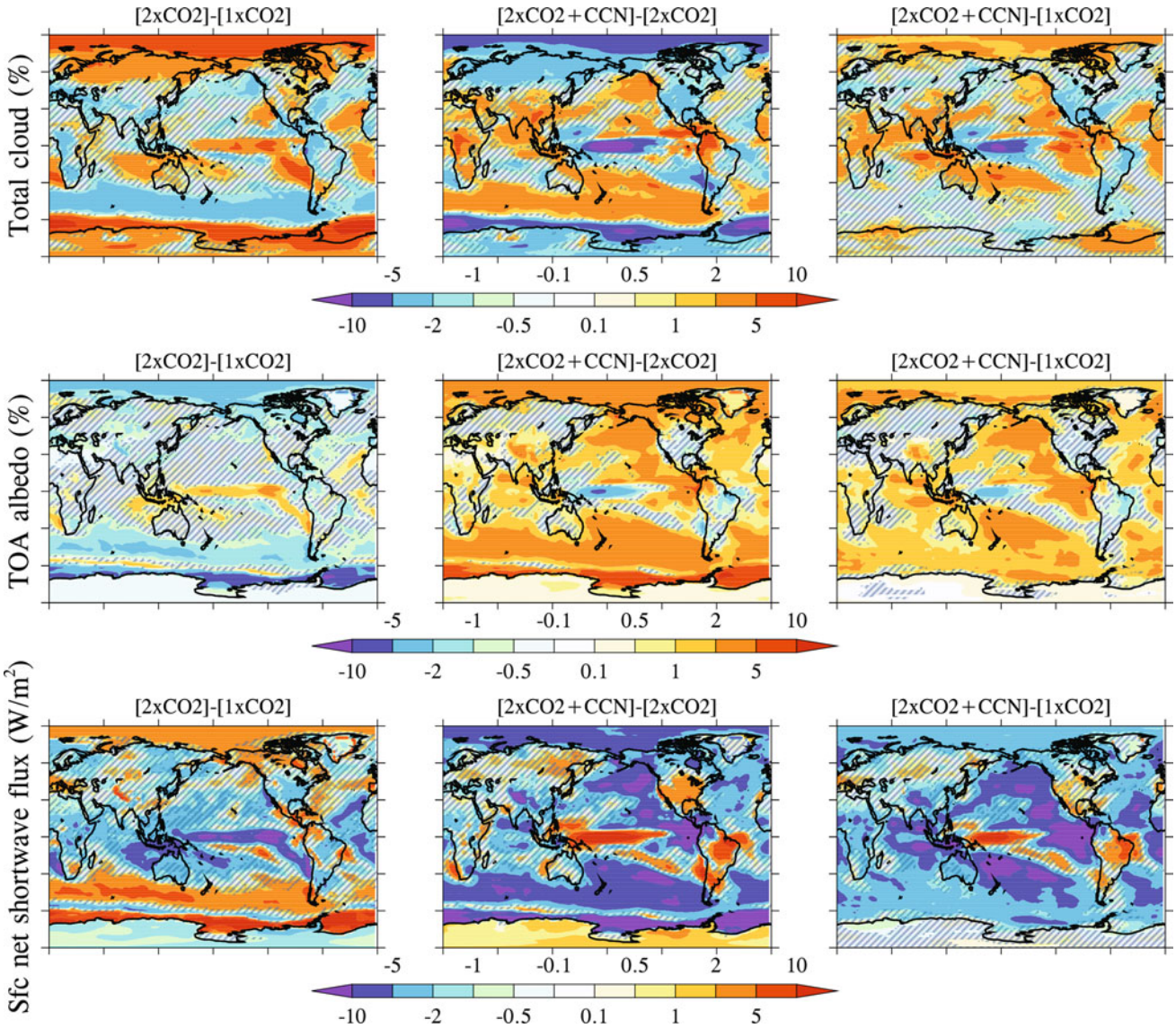

Fig. 6 Changes in global- and annual-mean total cloudiness, planetary albedo, and surface net shortwave radiation due to increase in CO_2 content ($2 \times CO_2 - 1 \times CO_2$), reduction in marine cloud droplet size ($2 \times CO_2 + CCN - 2 \times CO_2$) and a combination of both increased CO_2 content and reduced droplet size ($2 \times CO_2 + CCN - 1 \times CO_2$). Changes in cloudiness and albedo are absolute percentage changes. The hatching indicates regions where the changes are not significant at the 1% level. Significance level is estimated using a Student *t* test with a sample of 40 annual means and standard error corrected for autocorrelation (Zwiers and von Storch 1995). Cloud changes are significant at the 1% level over 51, 62 and 42% of globe, respectively, and TOA albedo and surface shortwave fluxes over 45, 76 and 66%, and 44, 60 and 62%, respectively

(P-E) over tropical land areas is increased. It should be noted the changes in precipitation, evaporation and P-E are dominated by small but significant areas (Fig. 7). This is especially true for P-E over land with significance at 1% level obtained for only 35, 39 and 22% of the land area for doubling of CO_2, reduction in marine cloud droplet size and for the combined effects, respectively.

Except for changes in surface temperature and precipitable water, changes for total clouds, TOA albedo, net surface solar fluxes precipitation, evaporation and precipitation minus evaporation are large (Figs. 5, 6, 7) for the combined effects of increased CO_2 content and decreased marine cloud droplet size (i.e., the $2 \times CO_2 + CCN$ simulation relative to the $1 \times CO_2$ simulation). This suggests that the residual regional changes are small only for surface temperature and water vapor; large regional changes in hydrology (precipitation, evaporation and runoff) are simulated. It should be noted that both precipitation and runoff show increases over land, particularly over India, Central America, Amazon and Sahel, in association with increased upward motion over tropical land (Fig. 4), suggesting that continents might not, on a mean basis, dry as a

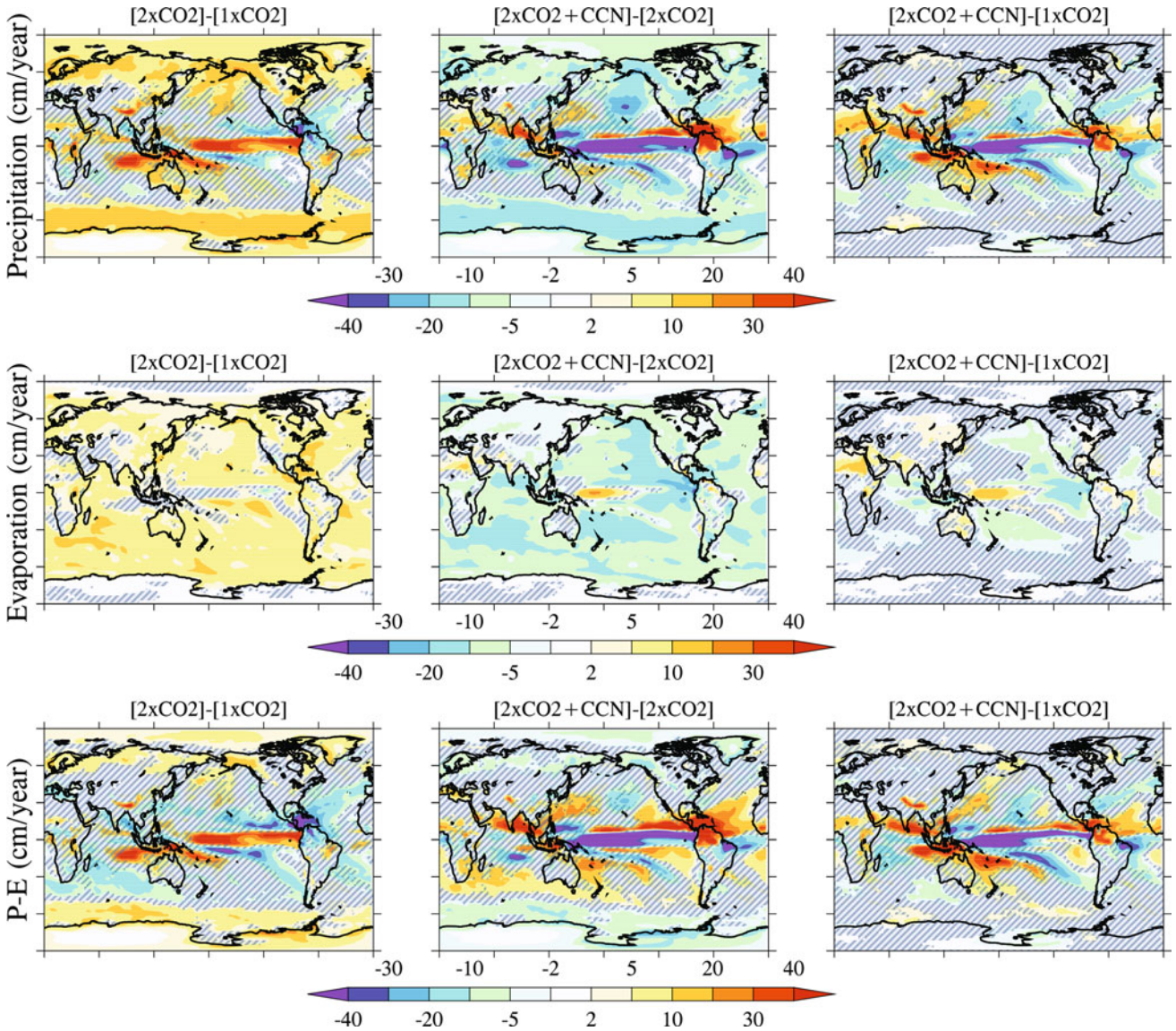

Fig. 7 Changes in global- and annual-mean precipitable water, precipitation (P), evaporation (E) and (P-E) due to increase in CO_2 content ($2 \times CO_2 - 1 \times CO_2$), reduction in marine cloud droplet size ($2 \times CO_2 + CCN - 2 \times CO_2$) and a combination of both increased CO_2 content and reduced droplet size ($2 \times CO_2 + CCN - 1 \times CO_2$). The hatching indicates regions where the changes are not significant at the 1% level. Significance level is estimated using a Student *t* test with a sample of 40 annual means and standard error corrected for autocorrelation (Zwiers and von Storch 1995). Precipitation changes are statistically significant at the 1% level over 46 (50), 58 (57), and 37 (31) % of the globe (land area) in the three comparisons, respectively. The corresponding fractions for evaporation are 85 (79), 89 (78) and 47 (44) % indicating higher confidence in evaporation changes. These fractions decrease to 39 (35), 46 (39) and 31 (22) % for (P-E), indicating slightly reduced confidence in regional scale changes in runoff

consequence of offsetting global warming by reducing marine cloud droplet size.

The zonal-mean changes in annual-mean surface temperature illustrate that most of the change in this field resulting from an increase in CO_2 are offset in the model by a decrease in marine cloud droplet size (Fig. 8): relative to $1 \times CO_2$, changes in the $2 \times CO_2 + CCN$ case are much smaller than that in the $2 \times CO_2$ case. However, large residual changes can be seen for the hydrological variables such as precipitation, evaporation and runoff for the combined effects of increased atmospheric CO_2 content and decreased marine cloud droplet size ($2 \times CO_2 + CCN - 1 \times CO_2$). Of particular interest here is the large increase in precipitation over tropical and southern hemisphere subtropical land areas in association with increased upward motion over land (Figs. 3, 4) while precipitation decreases over tropical oceans in this case. Evaporation also increases over these land regions but the magnitude of increases is smaller than precipitation. Hence, the runoff over land increases in the case with doubled CO_2 content

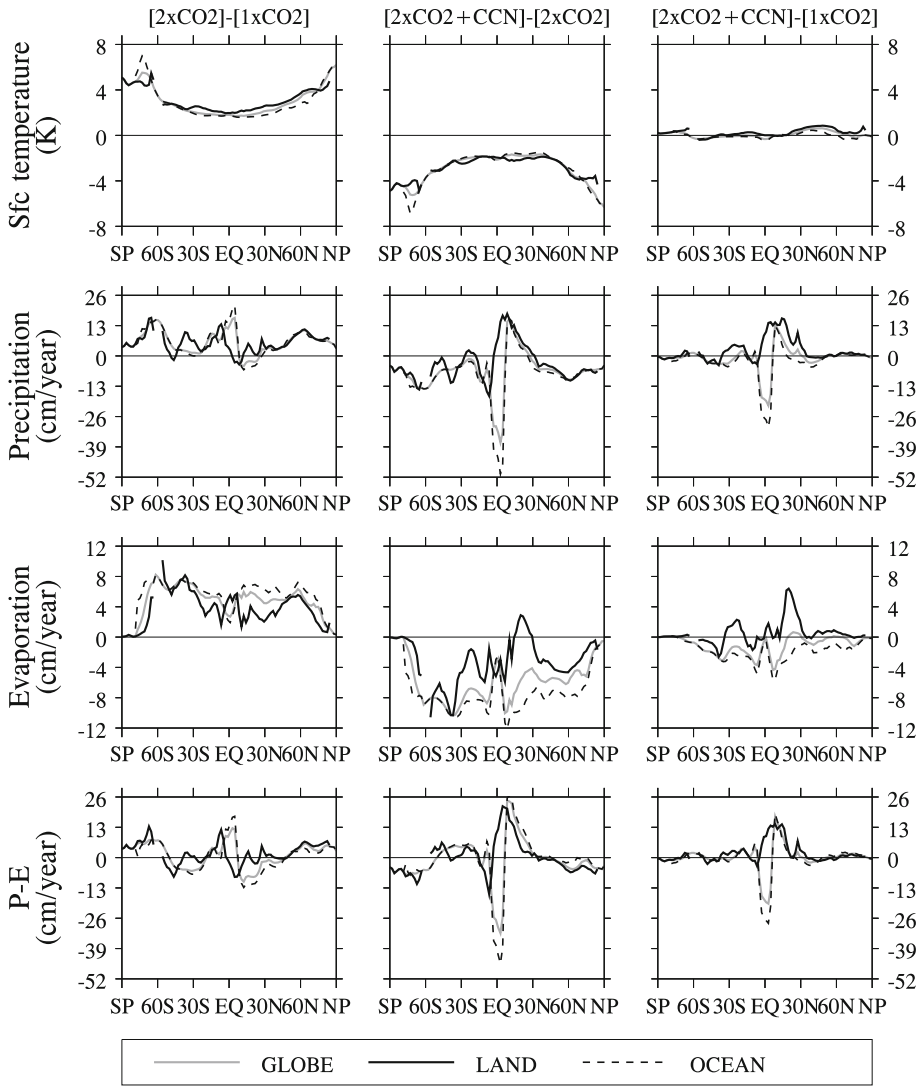

Fig. 8 Changes in zonal- and annual-mean surface temperature, precipitation (P), evaporation (E) and (P-E) due to increase in CO_2 content ($2 \times CO_2 - 1 \times CO_2$), reduction in marine cloud droplet size ($2 \times CO_2 + CCN - 2 \times CO_2$) and a combination of both increased CO_2 content and reduced droplet size ($2 \times CO_2 + CCN - 1 \times CO_2$) for land (*black*), ocean (*dashed*) and all regions (*gray*). Mitigation of climate change is achieved in terms of zonal-mean surface temperature changes in the case where both CO_2 is increased and cloud droplet size is reduced. However, large residual changes can be seen for the hydrological variables P, E and P-E. It should be noted that precipitation and runoff over land regions increase for this case, suggesting that offsetting of global warming by reducing marine cloud droplet size is unlikely, on average, to lead to a drying of the continent

and reduced marine cloud droplet size, and P-E decreases over oceans. Runoff increase over land and P-E (or freshwater flux) decrease over ocean occur simultaneously to close the land-sea water cycle.

4.4 Discussion on the vertical motion

When the marine cloud droplet radius is reduced, there is a reduction in solar radiative forcing over the oceans. After equilibrium climate change, we find that the net surface energy flux is nearly zero over both land and oceans (Table S1). This is expected because the climate system is in equilibrium, and hence land and ocean surfaces should have zero net surface flux. However, the top of atmosphere (TOA) net energy flux increases by 3.54 Wm^{-2} over land and decreases by 1.60 Wm^{-2} over oceans when the marine cloud droplet radius is reduced ($2 \times CO_2 + CCN - 2 \times CO_2$). This is primarily driven by applying a negative forcing only over oceans and is enhanced by climate feedbacks. This implies that there is a tendency for warming the atmospheric column over land and cooling over oceans. For equilibrium climate change, these temperature tendencies should be countered by sensible and latent heat transports from land to oceans and an associated secondary circulation that provides a net adiabatic cooling through upward motion over land and adiabatic warming through subsidence over oceans.

The upward motion can be diagnosed from the first law of thermodynamics (Holton 1992) which is given by

$$\frac{\partial T}{\partial t} = -\vec{V}_H \cdot \vec{\nabla}_H T - w\left(\frac{\partial T}{\partial z} + \Gamma_d\right) + Q \qquad (1)$$

where the first term on the right represents the horizontal advection of temperature, w is the vertical velocity, V_H is the horizontal wind velocity, Γ_d is the dry adiabatic lapse rate, $(\partial T/\partial z)$ is the environmental lapse rate, and Q is the diabatic heating rate. For equilibrium conditions, the left side of (1) vanishes. An upper bound on the vertical motion

can be obtained by applying (1) to a column of atmosphere averaged over land or oceans and omitting the horizontal advection:

$$w\left(\frac{\partial T}{\partial z}+\Gamma_d\right)=Q \quad (2)$$

Let us estimate the average vertical velocity over land when the marine cloud droplet radius is reduced ($2 \times CO_2 + CCN - 2 \times CO_2$). For illustrative purposes, we use $\partial T/\partial z = -7.5 \times 10^{-3}$ km^{-1} over land, and $\Gamma_d \sim 1.0 \times 10^{-4}$ km^{-1} (Holton 1992). We have used an environmental lapse rate over land that is between a dry and moist adiabat. The change in diabatic heating rate in the atmosphere is the change in net TOA energy flux since the change in surface net flux is nearly zero: Q = 3.5 Wm^{-2}/($M_{air} \times Cp_{air}$) where M_{air}($\sim 10^4$ kgm^{-2}) is the mass of air above a square meter and Cp_{air} ($\sim$1,000 J kg^{-1}K^{-1}) is the specific heat capacity of air. Substitution of the numerical values yields Q $\sim 3.5 \times 10^{-7}$ Ks^{-1}or $\sim 3.5 \times 10^{-2}$ K day^{-1}, and w $\sim$ 14 m day^{-1} or $\omega \sim -1.4$ mb day^{-1} in pressure coordinates where ω is the pressure velocity. This value agrees well with the value shown in Table 1 and Fig. 3 for the mid troposphere. When we apply (2) to the air column above ocean, we find that the magnitude of ω is about half of that over land and the sign is opposite. This is expected because land covers about 30% of the earth while oceans cover 70%, and the global mean of ω should be zero for mass conservation.

Application of (2) to the $2 \times CO_2 - 1 \times CO_2$ case similarly yields values of ω that approximately explain values listed in Table 1. A summation of results for $2 \times CO_2 + CCN - 2 \times CO_2$ and $2 \times CO_2 - 1 \times CO_2$ nearly explains changes observed in the $2 \times CO_2 + CCN - 1 \times CO_2$ case which has residual upward motion over land and downward motion over oceans (Table 1; Figs. 3, 4). We attribute the increased runoff over land to this residual upward motion over the tropical land (Fig. 4). A schematic diagram that illustrates the mass flux direction and horizontal heat fluxes in all the cases is shown in Fig. 9.

In the basic state ($1 \times CO_2$), the TOA net flux over land is -16.6 W m^{-2} and the ocean has an excess of about 7 Wm^{-2}. The net deficit over land is equal to about 2.5 peta Watts (PW) which is close to the observed value of 2.2 ± 0.1 PW (Fasullo and Trenberth 2008a) and the CMIP3 multi-model ensemble mean of 2.76 PW (Shin et al. 2006). This would suggest, based on the above analysis, that there is large upward motion over ocean and sinking motion over land. However, we find that the mean vertical motion over land and oceans are nearly zero (Table 1) but there is a large horizontal temperature difference ($\sim$8 K) between oceans and land (Table 1). In this case, horizontal heat transport between land and oceans balance the heat deficit over land and excess over the oceans (Fasullo and Trenberth 2008b; Lambert and Chiang 2007) with the associated averaged vertical motions over land and oceans in the secondary circulation being nearly zero.

5 Discussion

In this study, we have performed simulations using an atmospheric general circulation model (NCAR CAM3.5) coupled to a "slab" ocean model to investigate the potential for mitigation of climate change by altering the radius of marine cloud droplets. In these simulations the magnitude of the decrease in cloud droplet size was chosen to approximately offset the global mean warming from a doubling of atmospheric CO_2 content. Relative to the $1 \times CO_2$ control climate, the $2 \times CO_2$ climate with smaller cloud droplets ($2 \times CO_2 + CCN$) resulted in global land-mean precipitation increases of 3.52 ± 0.33% and runoff (precipitation minus evaporation) increases of 7.52 ± 0.87%. These results contrast with those from a previous study (Bala et al. 2008) which showed reduction in both precipitation and runoff over land for geoengineering schemes that deflect solar radiation above the tropopause without regard to the land/ocean distinction. The increase in runoff over land in this study occurs because the reduction of the droplet size of clouds and hence the enhancement of albedo is applied to clouds over only the ocean areas. This differential enhancement of cloud albedo leads to a monsoonal circulation with rising motion over land (Table 1; Figs. 3, 4, 9), and sinking motion over ocean with associated statistically significant increases in precipitation over land.

Reduction of the radius of marine cloud droplets from 14 to 11.5 μm ($2 \times CO_2 + CCN - 2 \times CO_2$) leads to a cooling of the ocean surface by 2.39 ± 0.03 K and 2.53 ± 0.04 K of the land surface; land surface temperatures decrease more than the ocean surface temperatures despite the fact that clouds are directly altered only over the ocean. This occurs because of differing lapse rates over oceans and land (Joshi and Gregory 2008; Joshi et al. 2008); on average, the atmosphere over the oceans has a moist adiabatic lapse rate but over land it has a lapse rate that is between a moist and dry lapse rates. Because of these differing lapse rates, temperature changes in the upper level are larger over the oceans than over land (Fig. 2); the atmospheric lapse rate change is larger for the atmosphere over oceans. Understanding temperature and hydrological changes over land surface requires a detailed investigation of climate responses on different time scales (Andrews et al. 2009; Bala et al. 2009). Such an investigation of the land surface hydrology will be the subject of a future paper.

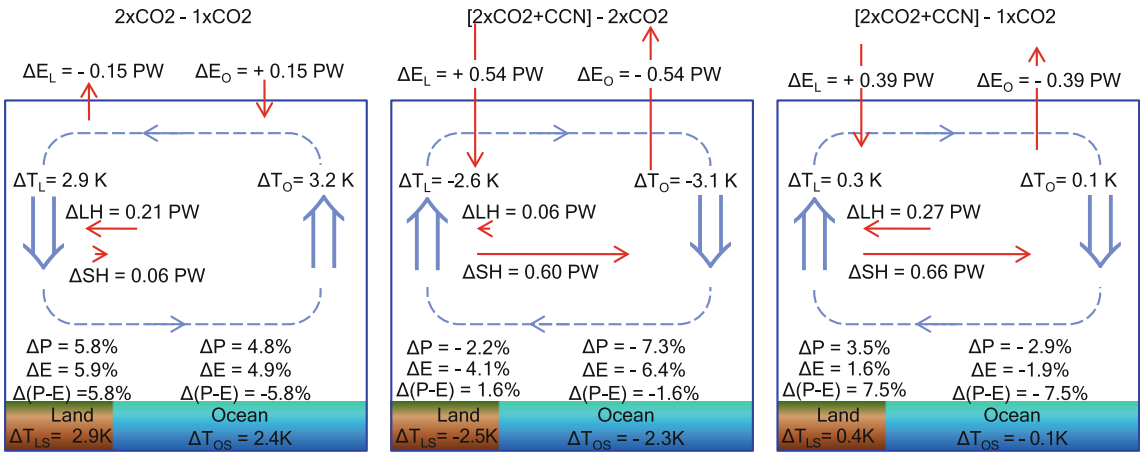

Fig. 9 Schematics that illustrates the changes in temperature, precipitation, evaporation, P-E, total energy, and mass and heat fluxes for doubled atmospheric CO_2 content ($2 \times CO_2 - 1 \times CO_2$) and reduced marine cloud droplet size ($2 \times CO_2 + CCN - 2 \times CO_2$) and the case where both the effects included ($2 \times CO_2 + CCN - 1 \times CO_2$). Circulation in blue shows the direction of atmospheric mass flow, the horizontal red arrows show the direction of sensible (SH) and latent heat (LH) fluxes, and ΔE_L and ΔE_O (*vertical red arrows*) show the gain or loss of energy for the column of air over land and oceans (gain is downward). The numerical values for all variables are taken or estimated from Table 1 and S1 except for SH transport which is inferred from ΔE_L, ΔE_O and LH transport. Temperatures changes in the upper level correspond to changes approximately at the 300 mb pressure level

While the surface warming and hydrological changes discussed in this study are caused by short and longwave radiative effects, they can be also caused by the possible impacts of the physiological effect of CO_2 on plant stomatal conductance called 'the CO_2 physiological forcing' (Betts et al. 2007; Boucher et al. 2009; Cao et al. 2009; Gedney et al. 2006). We note that these effects cannot be offset by a solar radiation management scheme. In order to isolate the radiative effects, we turned off the CO_2 physiological effect in this study.

The water budget over land is the result of a delicate balance between precipitation and surface evaporation. In this model, we have shown that the decrease in precipitation over land is smaller than the decrease in evaporation when the radius of marine cloud droplets is decreased, resulting in increased runoff over land. We have attributed this to an increased upward motion over land leading to less reduction in precipitation (see discussion in the Sect. 4.4). However, a large spread exists in climate models' precipitation responses to global warming (IPCC 2007). Therefore, it is critical to demonstrate if this result is robust across climate models. Are there any fundamental constraints on the transport of heat and water between land and oceans for increasing CO_2 and increased marine cloud albedo? Further theoretical and modelling studies on climate change and multi-model intercomparisons are required to address these questions.

In the real world, increased CCN could lead to smaller droplets which do not rain out as often because they do not reach "precipitable" raindrop sizes as quickly. Thus, not only does the decreased cloud droplet size lead to increased albedo, it also increases the lifetime of clouds. The increased lifetime could further increase the cloud-albedo and, therefore, the cloud life time effect could amplify the effect from the increase in cloud albedo. In our simulations, this effect of decreased cloud droplet size on cloud microphysics is not represented and, hence, the reduction in cloud droplet size need not be as large in real-world applications as in this study.

In the real world, it is probably impossible to seed clouds over all ocean areas, let alone uniform reduction in cloud droplet size. This approach would most likely, if at all, be deployed only for the persistent marine stratocumulus clouds off the west coasts of the continents such as South America, North America, Africa and Australia (Bower et al. 2006; Latham 1990, 2002; Latham et al. 2008). However, our aim here is not to predict consequences of particular possible deployments of this approach but rather to understand fundamental climate consequences of alteration of marine cloud albedo. Real-world cloud seeding schemes could affect the regional land water budgets, and thus much more detailed analysis would be required before large-scale deployment of such approaches could be seriously considered (Jones et al. 2009).

Caution should be exercised in interpreting our results because we have used a single atmospheric general circulation model coupled to a mixed layer ocean model. Transient responses and feedbacks from deep-ocean and dynamic sea-ice are not simulated in this study. Our simulations also lack many feedbacks associated with ocean and land biospheres. Other models could yield

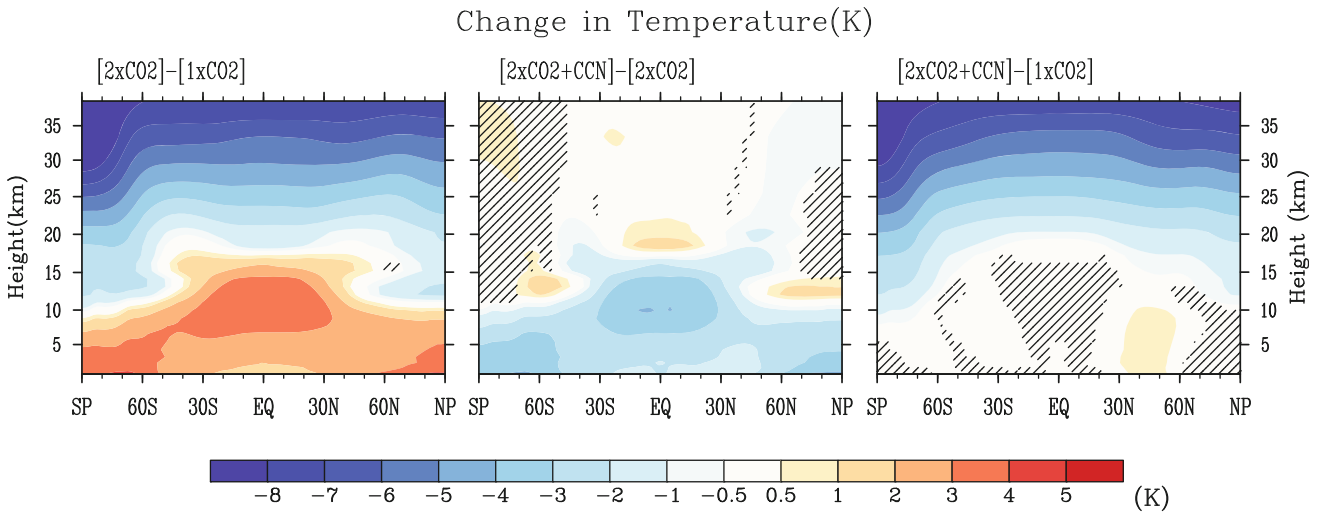

Fig. 10 Changes in zonally averaged global- and annual-mean temperature for the case with doubled atmospheric CO_2 content ($2 \times CO_2 - 1 \times CO_2$), reduced marine cloud droplet size ($2 \times CO_2 + CCN - 2 \times CO_2$) and the case where both the effects included ($2 \times CO_2 + CCN - 1 \times CO_2$). The hatching indicates regions where the changes are not significant at the 1% level. Significance level is estimated using a Student *t* test with a sample of 40 annual means and standard error corrected for autocorrelation (Zwiers and von Storch 1995). Warming is maximized near surface in the polar region and the tropical tropopause, and cooling is simulated in the stratosphere for the doubled CO_2 case. For the case with reduced marine cloud droplet size, there is cooling in the troposphere and little change in stratospheric temperatures. When both the effects are combined, the warming in the troposphere is mitigated but the cooling in the stratosphere is not mitigated indicating that the stratospheric climate change is not mitigated

quantitatively different results. Nonetheless, we believe that the basic qualitative results obtained here are robust and we recommend further studies on multi-model inter-comparisons to ensure this.

This study shows that enhancing the albedo of marine clouds could lead to increased runoff over land. Obviously, our model is much simpler than the real world, and in the real world, reducing marine cloud droplet size could have unforeseen consequences not anticipated by our model. There are enormous difficulties in untangling relationships among the aerosol, clouds and precipitation (Stevens and Feingold 2009). In the SRM scheme of seeding marine clouds that is considered in this study, the warming is mitigated in the troposphere but the cooling in the stratosphere is not mitigated indicating that the stratospheric climate change from increasing CO_2 is not mitigated (Fig. 10). This result is similar to conclusions from other studies that investigated the effects of reduced solar radiation above the tropopause without regard to land-sea contrasts to mitigate CO_2-induced climate change (Govindasamy and Caldeira 2000; Govindasamy et al. 2003). Clearly, SRM schemes, including the albedo-enhancement of marine clouds, will leave the ocean acidification problem unsolved (Mathews et al. 2009). If we commit to any SRM scheme, in the absence of active removal of greenhouse gases from the atmosphere, we may be committing to that scheme for multiple centuries (Bengtsson 2006). It may be difficult to develop and maintain over centuries an international consensus to engage in a large-scale geoengineering project (Schneider 2001). Failure of a stabilization scheme could be catastrophic (Matthews and Caldeira 2007). Therefore, a careful integrated assessment is required before committing to any geoengineering scheme.

In summary, prior studies have suggested that offsetting global warming by reflecting sunlight to space would result in a drying of the continents. In contrast, our study indicates that reflecting sunlight to space by reducing cloud droplet size over the oceans could lead, on average, to a moistening of the continents.

Acknowledgments We thank Prof. J. Srinivasan of Divecha Center for Climate Change, Indian Institute of Science for suggestions which helped to improve this manuscript.

References

Allen MR, Ingram WJ (2002) Constraints on future changes in climate and the hydrologic cycle. Nature 419(6903):224–232

Andrews T, Forster PM, Gregory JM (2009) A surface energy perspective on climate change. J Clim 22:2557–2570

Angel R (2006) Feasibility of cooling the earth with a cloud of small spacecraft near the inner Lagrange point (L1). Proc Natl Acad Sci USA 103(46):17184–17189

Bala G (2009) Problems with geoengineering schemes to combat climate change. Curr Sci 96(1):41–48

Bala G, Duffy PB, Taylor KE (2008) Impact of geoengineering schemes on the global hydrological cycle. Proc Natl Acad Sci USA 105(22):7664–7669

Bala G, Caldeira K, Nemani R (2009) Fast versus slow response in climate change: implications for the global hydrological cycle. Clim Dyn. doi:10.1007/s00382-009-0583-y

Bengtsson L (2006) Geo-engineering to confine climate change: is it at all feasible? Clim Change 77(3–4):229–234

Betts RA et al (2007) Projected increase in continental runoff due to plant responses to increasing carbon dioxide. Nature 448(7157):U5–U1037

Boucher O, Jones A, Betts RA (2009) Climate response to the physiological impact of carbon dioxide on plants in the Met Office Unified Model HadCM3. Clim Dyn 32(2–3):237–249

Bower K, Choularton T, Latham J, Sahraei J, Salter S (2006) Computational assessment of a proposed technique for global warming mitigation via albedo-enhancement of marine stratocumulus clouds. Atmos Res 82(1–2):328–336

Cao L, Bala G, Caldeira K, Nemani R, Ban-Weiss G (2009) Climate response to physiological forcing of carbon dioxide simulated by the coupled community atmosphere model (CAM3.1) and community land model (CLM3.0). Geophys Res Lett 36:L10402. doi:10.1029/2009GL037724

Collins WD et al (2006) The formulation and atmospheric simulation of the community atmosphere model version 3 (CAM3). J Clim 19(11):2144–2161

Crutzen PJ (2006) Albedo enhancement by stratospheric sulfur injections: a contribution to resolve a policy dilemma? Clim Change 77(3–4):211–219

Doutriaux-Boucher M, Webb MJ, Gregory JM, Boucher O (2009) Carbon dioxide induced stomatal closure increases radiative forcing via a rapid reduction in low cloud. Geophys Res Lett 36

Early JT (1989) The space based solar shield to offset greenhouse effect. J Br Interplanet Soc 42:567–569

Fasullo JT, Trenberth KE (2008a) The annual cycle of the energy budget. Part I: global mean and land-ocean exchanges. J Clim 21(10):2297–2312

Fasullo JT, Trenberth KE (2008b) The annual cycle of the energy budget. Part II: meridional structures and poleward transports. J Clim 21(10):2313–2325

Forster PM, Blackburn M, Glover R, Shine KP (2000) An examination of climate sensitivity for idealised climate change experiments in an intermediate general circulation model. Clim Dyn 16(10–11):833–849

Gedney N et al (2006) Detection of a direct carbon dioxide effect in continental river runoff records. Nature 439(7078):835–838

Govindasamy B, Caldeira K (2000) Geoengineering earth's radiation balance to mitigate CO_2-induced climate change. Geophys Res Lett 27(14):2141–2144

Govindasamy B, Thompson S, Duffy PB, Caldeira K, Delire C (2002) Impact of geoengineering schemes on the terrestrial biosphere. Geophys Res Lett 29(22):2061. doi:10.1029/2002GL015911

Govindasamy B, Caldeira K, Duffy PB (2003) Geoengineering earth's radiation balance to mitigate climate change from a quadrupling of CO_2. Glob Planet Change 37(1–2):157–168

Gregory J, Webb M (2008) Tropospheric adjustment induces a cloud component in CO_2 forcing. J Clim 21(1):58–71

Gregory JM et al (2004) A new method for diagnosing radiative forcing and climate sensitivity. Geophys Res Lett 31(3):L03205. doi:10.1029/2003GL018747

Hansen J, Sato M, Ruedy R (1997) Radiative forcing and climate response. J Geophys Res Atmos 102(D6):6831–6864

Hansen J et al (2005) Efficacy of climate forcings. J Geophys Res Atmos 110(D18):D18104. doi:10.1029/2005JD005776

Held IM, Soden BJ (2006) Robust responses of the hydrological cycle to global warming. J Clim 19(21):5686–5699

Holton J (1992) An introduction to dynamics meteorology, 5th edn. Academic Press, New York, USA, p 511

IPCC (2007) Climate change 2007: the physical science basis. Contribution of working group I to the fourth assessment report of the intergovernmental panel on climate change. Cambridge University Press, Cambridge, UK and New York, NY, USA

Jones A, Haywood J, Boucher O (2009) Climate impacts of geoengineering marine stratocumulus clouds. J Geophys Res Atmos 114:D10106. doi:10.1029/2008JD011450

Joshi M, Gregory J (2008) Dependence of the land-sea contrast in surface climate response on the nature of the forcing. Geophys Res Lett 35(24)

Joshi MM, Gregory JM, Webb MJ, Sexton DMH, Johns TC (2008) Mechanisms for the land/sea warming contrast exhibited by simulations of climate change. Clim Dyn 30(5):455–465

Lambert FH, Chiang JCH (2007) Control of land-ocean temperature contrast by ocean heat uptake. Geophys Res Lett 34(13)

Latham J (1990) Control of global warming. Nature 347(6291):339–340

Latham J (2002) Amelioration of global warming by controlled enhancement of the albedo and longevity of low-level maritime clouds. Atmos Sci Lett. doi:10.1006/Asle.2002.0048

Latham J et al (2008) Global temperature stabilization via controlled albedo enhancement of low-level maritime clouds. Philos Trans Roy Soc Math Phys Eng Sci 366(1882):3969–3987

Lunt DJ, Ridgwell A, Valdes PJ, Seale A (2008) "Sunshade World": a fully coupled GCM evaluation of the climatic impacts of geoengineering. Geophys Res Lett 35(12):L12710. doi:10.1029/2008GL033674

Mathews D, Cao L, Caldeira K (2009) Sensitivity of ocean acidification to geoengineered climate stabilization. Geophys Res Lett 36:L10706. doi:10.1029/2009GL037488

Matthews HD, Caldeira K (2007) Transient climate-carbon simulations of planetary geoengineering. Proc Natl Acad Sci USA 104(24):9949–9954

NAS 1992 (1992) Policy implications of greenhouse warming: mitigation, adaptation and the science base. National Academy of Sciences. National Academy Press, Washington ,DC, Chap. 28 (Geoengineering), pp 433–464

Oleson KW, et al (2008) Improvements to the Community Land Model and their impact on the hydrological cycle. J Geophys Res Biogeosci 113(G1)

Rasch PJ, Crutzen PJ, Coleman DB (2008) Exploring the geoengineering of climate using stratospheric sulfate aerosols: the role of particle size. Geophys Res Lett 35(2):L02809. doi:10.1029/2007GL032179

Robock A, Oman L, Stenchikov GL (2008) Regional climate responses to geoengineering with tropical and Arctic SO2 injections. J Geophys Res 113:D16101. doi:10.1029/2008JD010050

Schneider SH (2001) Earth systems engineering and management. Nat 409(6818):417–421

Seifritz W (1989) Mirrors to halt global warming. Nature 340(6235):603

Shin HJ, Chung IU, Kim HJ, Kim JW (2006) Global energy cycle between land and ocean in the simulated 20th century climate systems. Geophys Res Lett 33(14)

Stevens B, Feingold G (2009) Untangling aerosol effects on clouds and precipitation in a buffered system. Nature 461:607–613

Sutton RT, Dong BW, Gregory JM (2007) Land/sea warming ratio in response to climate change: IPCC AR4 model results and comparison with observations. Geophys Res Lett 34(2):L02701. doi:10.1029/2006GL028164

Teller E, Wood L, Hyde R (1997) Global warming and ice ages: I. Prospects for physics based modulation of global change, UCRL-231636/UCRL JC 128715. Lawrence Livermore National Laboratory, Livermore, CA, USA

Tilmes S, Garcia RR, Kinnison DE, Gettelman A, Rasch P (2009) Impact of geoengineered aerosols on the troposphere and stratosphere. Geophys Res Lett 114:D12305. doi:10.1029/2008JD011420

Trenberth KE, Dai A (2007) Effects of mount Pinatubo volcanic eruption on the hydrological cycle as an analog of geoengineering. Geophys Res Lett 34(15):L15702. doi:10.1029/2007GL030524

Twomey S (1977) Influence of pollution on shortwave albedo of clouds. J Atmos Sci 34(7):1149–1152

Zwiers F, von Storch H (1995) Taking serial correlation into account in tests of the mean. J Clim 8:336–351